

PAPER

Ga metal nanoparticle-GaAs quantum molecule complexes for terahertz generation

To cite this article: Sergio Bietti *et al* 2018 *Nanotechnology* **29** 365602

View the [article online](#) for updates and enhancements.

Related content

- [Crystallization kinetics of Ga metallic nano-droplets under As flux](#)
S Bietti, C Somaschini and S Sanguinetti
- [Droplet epitaxy for advanced optoelectronic materials and devices](#)
Jiang Wu and Zhiming M Wang
- [Control of the lateral growth morphology in GaAs Droplet Epitaxy](#)
C Somaschini, S Bietti, S Sanguinetti et al.





IOP | ebooks™

Bringing you innovative digital publishing with leading voices to create your essential collection of books in STEM research.

Start exploring the collection - download the first chapter of every title for free.

Ga metal nanoparticle-GaAs quantum molecule complexes for terahertz generation

Sergio Bietti¹ , Francesco Basso Basset¹, David Scarpellini¹, Alexey Fedorov², Andrea Ballabio¹, Luca Esposito³, Martin Elborg⁴, Takashi Kuroda⁴, Ákos Nemcsics⁵, Lajos Tóth⁶, Cristian Manzoni⁷, Caterina Vozzi⁷  and Stefano Sanguinetti¹

¹ L-NESS and Dipartimento di Scienza dei Materiali, Università di Milano-Bicocca, via Cozzi 53, I-20125 Milano, Italy

² CNR-IFN and L-NESS, via Anzani 42, I-22100 Como, Italy

³ L-NESS and Politecnico di Milano, via Anzani 42, I-22100 Como, Italy

⁴ National Institute for Materials Science, 1-2-1 Sengen, Tsukuba, Ibaraki 305-0047, Japan

⁵ Institute of Microelectronics and Technology, Óbuda University and MFA, Tavaszmező u. 17, H-1084 Budapest, Hungary

⁶ MTA-EK-MFA, H-1525 Budapest Pf. 49, Hungary

⁷ CNR Istituto di Fotonica e Nanotecnologie, Piazza Leonardo da Vinci 32, I-20133 Milano, Italy

E-mail: sergio.bietti@mater.unimib.it

Received 5 April 2018, revised 1 June 2018

Accepted for publication 18 June 2018

Published 2 July 2018



Abstract

A hybrid metal–semiconductor nanosystem for the generation of THz radiation, based on the fabrication of GaAs quantum molecules-Ga metal nanoparticles complexes through a self assembly approach, is proposed. The role of the growth parameters, the substrate temperature, the Ga and As flux during the quantum dot molecule (QDM) fabrication and the metal nanoparticle alignment are discussed. The tuning of the relative positioning of QDMs and metal nanoparticles is obtained through the careful control of Ga droplet nucleation sites via Ga surface diffusion. The electronic structure of a typical QDM was evaluated on the base of the morphological characterizations performed by atomic force microscopy and cross sectional scanning electron microscopy, and the predicted results confirmed by micro-photoluminescence experiments, showing that the Ga metal nanoparticle-GaAs quantum molecule complexes are suitable for terahertz generation from intraband transition.

Keywords: droplet epitaxy, nano-positioning, molecular beam epitaxy, atomic force microscopy, quantum nanostructures, III–V semiconductors

(Some figures may appear in colour only in the online journal)

Efficient generation of radiation in the terahertz frequency range (0.3–10 THz) has recently attracted considerable interest due to some important possible applications, such as the increased speed of data transfer via wireless route and the identification of large complex molecules to perform environmental analysis, security screening applications, non-invasive biomedical imaging and medical tomography, manipulation of charged and magnetic particles and nanoparticles [1–7]. The use of metal nanoparticles (MNs) to enhance emission rates of quantum emitters was recently studied for different nanohybrid systems [8, 9], and in particular addressed for medical applications [10–12].

A very promising mechanism proposed to generate coherent THz radiation is based on bound-bound transitions in quantum nanostructures when irradiated by femtosecond laser pulses [13]. A recent theoretical investigation [14] has suggested that high efficiency sources can be realized by nano-engineered semiconductor surfaces, where specially designed hybrid resonant plasmon-exciton systems composed by quantum dot molecules (QDMs) and MNs are fabricated. QDMs should be carefully designed to provide a three-level Λ -type system in which the two lowest lying levels are localized in different spatial regions, and their energy

separation makes the bound-bound transition suitable for THz generation [15, 16]. MNs should be accurately positioned so that their surface plasmon oscillation enhances the electric field in the QDM leading to a higher probability of difference-frequency generation [14]. In particular, the positioning of the Ga droplet in between the two quantum dots of the QDM is expected to maximize the plasmonic resonance effects of the THz emission of the system [14].

In order to achieve the required control of the quantum nanostructure morphology and the self-alignment of MNs with the QDMs, we present a self assembly procedure based on droplet epitaxy (DE). DE is a versatile technique, totally performed in MBE environment, for the growth of high quality III–V quantum nanostructures introduced by Dr Nobuyuki Koguchi in 1991 [17, 18]. It consists in two separate steps: in the first one, metal nano-droplets formed by group III atoms are deposited with small size dispersion on the substrate. The second step provides group V element to crystallize the metallic droplets into complex III–V nanostructures. Depending on the crystallization conditions, the fabricated nanostructure morphology can be tuned among dot, ring, disks and other combinations [19, 20]. Taking advantage on the different diffusion length of Ga adatoms along the [01-1] and the [011] directions [21, 22], it is also possible to obtain QDM nanostructures [23–25] whose morphology can be tailored to provide a three-level Λ -type system. The same metallic Ga nano-droplets, which can self-assembled by MBE on the Ga(Al)As surface as the starting point of DE, are good candidates for MN in resonance with the Ga(Al)As QDM transitions, as Ga nanoparticles show a wide plasmonic resonance extending in the near infrared [26–28].

1. Experimental details

The growth experiments were performed in a conventional MBE system (Veeco Gen II), on epi-ready GaAs (001) substrates. For optimal control of the As flux during the growth, a valved cell was used. The cracking zone temperature of the As cell was set at 600 °C in order to provide As₄ molecules in every experiment. Sample growth experiments were monitored *in situ* by reflection high-energy electron diffraction (RHEED).

After the oxide desorption at 580 °C, an atomically smooth surface was prepared by growing a 150 nm thick GaAs buffer layer and a 70 nm Al_{0.3}Ga_{0.7}As barrier layer. The substrate temperature was then decreased to 340 °C and the As valve closed at 420 °C in order to deplete the growth chamber of the arsenic molecules. At this point, the RHEED pattern clearly showed a $c(4 \times 4)$ surface reconstruction. The growth of the QDP-MN complexes is performed in two steps. In the first one, by means of DE, a QDM with the requested morphology is realized. In the second, a Ga MN is positioned, by capillarity and diffusion processes, on the top of the QDM. QDM fabrication proceeded as follows: when the background pressure reached a saturation value below 5×10^{-10} Torr, an equivalent amount of 1.05 MLs of Ga with a deposition rate of 0.03 ML s⁻¹ was supplied to the substrate surface to form

Ga droplets at the same temperature. During the Ga supply, the surface reconstruction changed to (4×6) Ga-rich reconstruction [29] after the deposition of 1.0 MLs of Ga. Continuing with the deposition of Ga, no further changes in the surface reconstruction are observed. The Ga deposited in excess of 1 ML then results in the nucleation of Ga droplets on the surface, whose density is determined by the temperature of the substrate and by the Ga flux [30].

The substrate temperature was then decreased to 230 °C and the Ga droplets irradiated with an As flux with a beam equivalent pressure of 7×10^{-6} Torr for 5 min. The RHEED pattern slowly changed to spotty due to the crystallization of the Ga droplets into GaAs nanostructures.

The sample was then annealed for 5 min at 380 °C in As flux in order to improve the QDM crystalline quality while maintaining low changes in the nanostructure morphologies [31, 32]. No change in the RHEED pattern was observed. Sample A was removed from the chamber at this growth stage.

In order to study the influence of the substrate temperature on the positioning of Ga droplets we deposited 1.8 MLs of Ga with a rate of 0.03 ML s⁻¹ on the GaAs nanostructures at 320 °C, 340 °C and 360 °C on samples B1, B2 and B3 respectively. In order to study the influence of the Ga flux, we deposited 1.8 MLs of Ga with a rate of 0.05 ML s⁻¹ on the GaAs nanostructures at 360 °C on samples C. On these four samples the Ga deposition for the formation of MN was performed after closing the As valve with a background pressure below 5×10^{-10} Torr. The As valve was closed in each experiment at the same temperature of Ga droplet deposition.

The morphological characterization of the samples was performed *ex situ* by an atomic force microscope (AFM) and high resolution transmission electron microscopy (HR-TEM). Veeco Innova AFM was used in tapping mode with ultra-sharp tips capable of a lateral resolution of about 2 nm. Thin cross sectional specimens from the sample were prepared for the TEM investigations by cutting, embedding into a special holder, mechanical grinding, polishing, and finally ion beam milled with 10 keV Ar ions. The conventional TEM imaging of the samples was performed on a Philips CM20 electron-microscope at 200 kV. The high resolution images were taken with 300 kV JEOL 3010 high resolution microscope.

Micro-photoluminescence (μ -PL) measurements were performed using a continuous wave diode-pumped laser with a wavelength of 532 nm as an excitation source. The laser beam was focused on the sample surface with a spot size of 1.5 μ m in diameter. The PL signal was collected by an objective lens with a numerical aperture of 0.55 (Nikon LCD Plan 50x), fed into a polychromator with a focusing length of 50 cm and spectrally analyzed by a charge-coupled detector. The μ -PL measurements were performed at 11 K.

2. Results and discussion

Figure 1(a), shows a $1 \times 1 \mu\text{m}^2$ AFM scan of the surface of sample A after the growth, confirming the presence of QDMs.

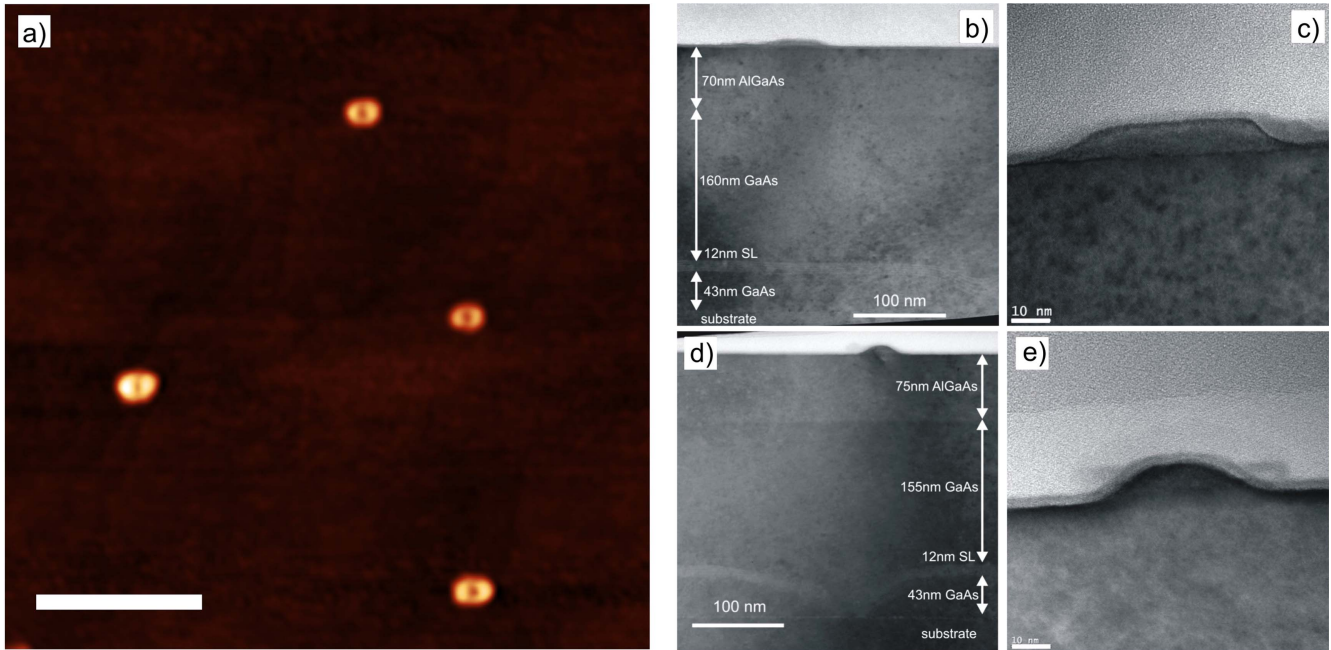


Figure 1. Panel (a) $1 \times 1 \mu\text{m}^2$ AFM scan of the surface of sample A. White bar is 250 nm long. Panels (b)–(e) show cross sectional HR-TEM images of the sample. Panels (c) and (e) show a magnified picture of the same nanostructures as in panels (b) and (d), respectively.

The peculiar shape of the nanostructures is due to anisotropic gallium adatoms diffusion along the [01-1] direction compared with [011] [23–25]. The density of the nanostructures is $3.8 \times 10^{-8} \text{ cm}^{-2}$, the mean length of major and minor axes are 75 and 55 nm respectively, the mean height of the two quantum dots forming each pair is approximately 9 and 8.5 nm. Although the elongation of the nanostructure is always along [01-1] direction, the position of the highest peak in the nanostructure can be exchanged.

The conventional and the HR-TEM pictures of the nanostructures are shown across two planes perpendicular to each other. Panels (b)–(e) of figure 1 show the sample cut along [011] (panels (b) and (c)) and [01-1] (panels (d) and (e)) directions, respectively. Panels (c) and (e) show the same nanostructure of panels (b) and (d), respectively, with different magnification. The cross sectional high resolution TEM images of the DE nanostructure demonstrate its perfect crystallinity. The crystal planes of the substrate are continued without any break in the nanostructure, no defects can be observed at the interface.

The electronic structure of a typical QDM was evaluated by using a single-band, constant-potential numerical model. The computational method is based on the approach developed by Califano and Harrison [33] and applies conveniently to strain-free quantum dots, since reliable effective mass parameters are known [19]. Due to the modest computational requirements of the model, it was possible to relax any assumption on the shape symmetry and use the exact geometry probed by the AFM scans prior to the deposition of the MNs. The electronic structure of the QDM was evaluated without considering the presence of the MN. The energy shift

of the excitonic transitions due to the dipole–dipole coupling with the MN is expected to be a minor contribution with respect to the accuracy required for this calculation [34]. The Schrödinger equation for the envelope function in the effective mass approximation was expanded on a basis of 33 wave functions in each direction and diagonalized in order to obtain both the electron and the hole energy eigenstates and eigenvalues. In particular, the simulation estimated the energy separation between the two lowest lying confined states, together with their spatial distribution in the QDM. The probability to find the electron wave function inside the QDM structure was illustrated in figure 2. The ground and the first excited electron state are localized in the smaller and the bigger dome of the QDM respectively. The energy separation between these two levels is approximately 12 meV, which matches an interesting portion of the THz gap around 3 THz. On the other hand, the energy separation between the two lowest lying heavy-hole states is only 2.5 meV, lower than the line broadening at room temperature due to the elastic scattering with acoustic photons [35]. Assuming that the Coulomb interaction does not dramatically affect this energy separation, the hole state is effectively not localized in the excitonic complex with an electron in each of the two confined states of the bound-bound transition. A three-level Λ -type system is achieved so that the QDM ensemble meets the requirements for the emission of radiation in the THz range [14].

Figure 3 shows the μ -PL spectra of GaAs QDMs. The sample used for this analysis is equivalent with sample A listed in table 1. It consists of GaAs QDM without self-aligned Ga metal particles. The main difference is in the

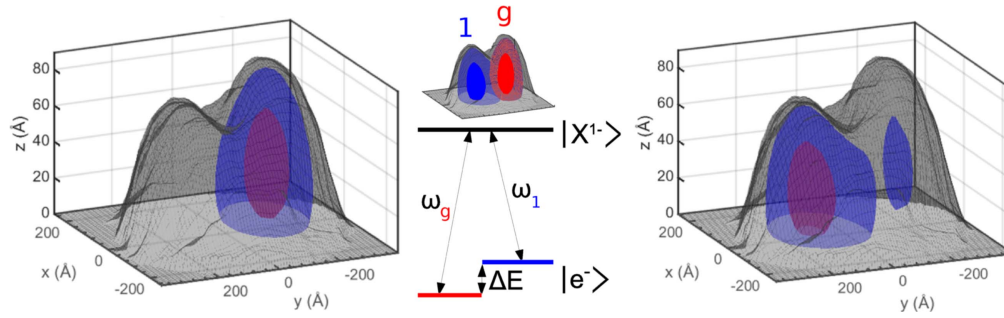


Figure 2. Left and right panels: probability density isosurfaces (50% red, 95% blue) of the envelope function of the electron wave function confined inside a QDM structure, ground (left panel) and first excited (right panel) state. In the central panel, schematic drawing of three-level Λ -type system of the single QDM, where g (red) indicates the the ground electronic state and 1 (blue) the first excited electronic state, ΔE is the energy separation between these two levels, ω_g and ω_1 are the frequency separation between the upper charged exciton state and the ground or the first excited electronic state, respectively.

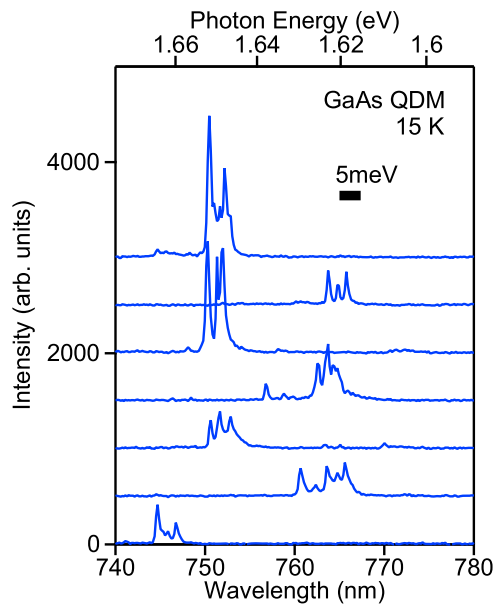


Figure 3. μ -PL measurements of different single QDMs showing a splitting energy of several meV in agreement with theoretical calculations. Each QDM exhibits the spectral multiplet even at a low excitation limit, and was thus attributed to different single-particle levels.

Table 1. Substrate temperature and Ga flux of fabricated samples for the QDM formation and the MN deposition.

Sample	Substr. temp.	Ga flux	Substr. temp.	Ga flux
	QDM ($^{\circ}\text{C}$)	QDM (ML s^{-1})	MN ($^{\circ}\text{C}$)	MN (ML s^{-1})
A	340	0.03	—	—
B1	340	0.03	320	0.03
B2	340	0.03	340	0.03
B3	340	0.03	360	0.03
C	340	0.03	360	0.05

presence a of 50 nm $\text{Al}_{0.3}\text{Ga}_{0.7}\text{As}$ barrier layer followed by 5 nm GaAs capping layer, which efficiently blocked non-radiative recombination, and enhanced the PL efficiency. The PL signals of GaAs QDM are identified at a spectral range

between 740 and 770 nm (1.6–1.7 eV), which agrees with transition energies predicted by the single-band calculations. The PL spectra of isolated QDM are characterized by the co-presence of multiple lines, whose appearance is independent of excitation densities. Moreover, each QDM exhibits the spectral multiplet even at a low excitation limit, where the average number of photoinjected carriers is less than one. This spectral signature is in stark contrast to the PL spectra of standard lens-like GaAs quantum dots, which exhibit density-dependent multiexciton lines [36]. The spectral multiplets of QDM are therefore attributed to different single-particle levels. Thanks to the large volume of QDM, energy splittings between different confinement levels are several meV, suitable for THz radiation. The order of the spectral lines and their splitting energy show some variations from one single QDM to another, as the single-particle levels are sensitive to the microscopic shape. The observed splitting energies are distributed from 2 to 8 meV, which agrees with the calculated single-particle splitting of heavy holes (2.5 meV) and that of electrons (12 meV, as discussed before). The coherent excitation of split electron levels is expected to drive THz radiation.

The results of the deposition of the Ga MNs on the QDMs with different substrate temperatures and a fixed flux of 0.03 ML s^{-1} is shown in figure 4. While the parameters for the fabrication of the QDMs were not changed, leading to the formation of the same nanostructures with similar density on each sample, the different temperatures used during the Ga MNs formation lead to different effects, as shown in figures 4(a)–(c). The first effect is a change in the MN density, as expected in DE process. The density of the Ga droplets on the surface decreases as the substrate temperature is increased, as already reported in [37, 38]. This means that the density of MNs is decreasing while increasing the substrate temperature thus the density of the MNs, compared to the one of the QDMs (deposited at 340°C on all the samples), is higher for sample B1, similar for sample B2 and lower for sample B3. The second effect is related to the size of the Ga MNs. To explain this behavior, again we have to consider the dependence of Ga MN density on substrate temperature and the effect of surface reconstruction. On one side, increasing the density of Ga MN keeping unchanged the amount of Ga

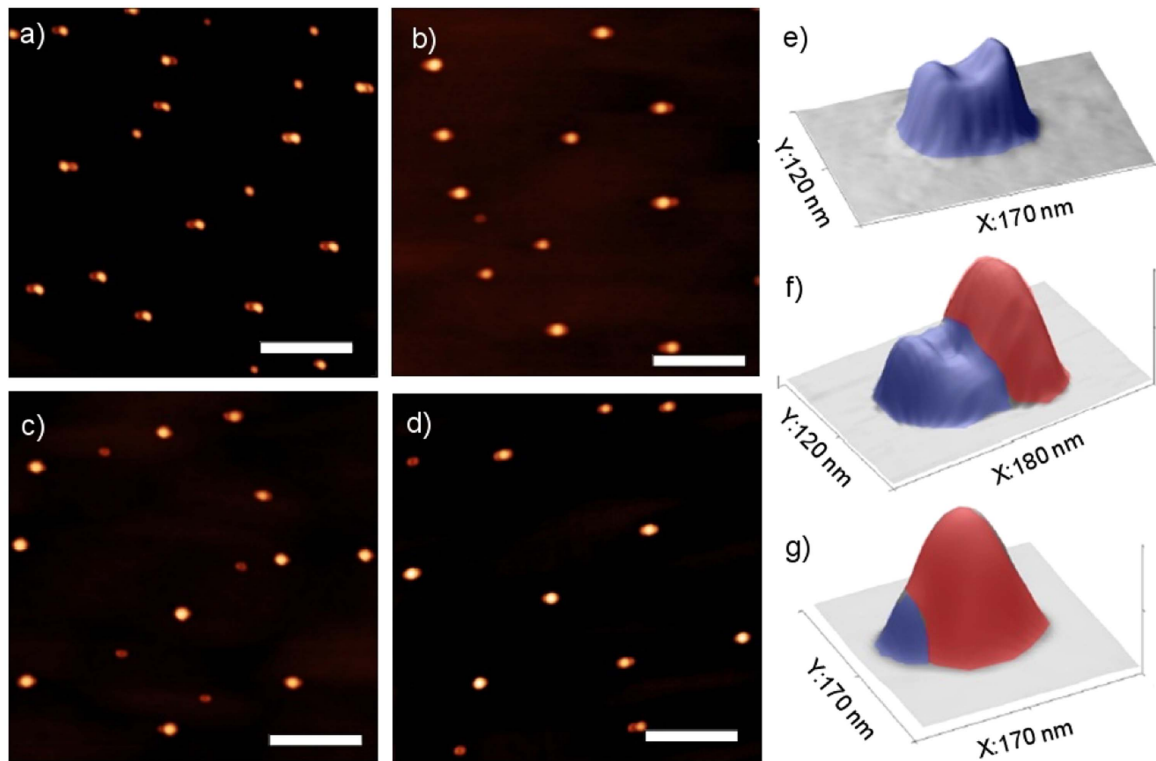


Figure 4. $2 \times 2 \mu\text{m}^2$ AFM scans of the surface of sample B1, B2 and B3 (panels (a)–(c) respectively) and of sample C (panel (d)). White bars are 500 nm long. Panels (e)–(g) report tridimensional magnifications of single QDM without MN, with MN formed next to and on top of it, respectively. Red and blue colors are used to highlight the MN and QDM, respectively.

deposited, lead to the formation of smaller droplets. On the other side, we have to consider that while the RHEED pattern shows a $c(4 \times 4)$ surface reconstruction for all the samples, closing the As valve at different substrate temperatures leads to the formation on the surface of a different excess of As before the Ga deposition. This effect is due to the presence of the two phases of $c(4 \times 4)$ surface reconstruction, the $c(4 \times 4)\alpha$ and the $c(4 \times 4)\beta$ with an excess of As of 1.0 and 1.75 MLs, respectively [39]. Increasing the substrate temperature results in a reduction of the As excess on the surface and, consequently, in a larger amount of Ga available for the Ga MN formation.

The third and most relevant effect in this sample series is the dependence on temperature of the droplet position with respect to the QDM, as the nano-positioning of the MNs in between the two quantum dots of the QDM is expected to maximize the plasmonic resonance effects of the THz emission of the system [14]. At low T (sample B1) the Ga MNs mostly form next to each QDM along the [01-1] direction and only a small fraction on top, as shown in panel (a) of figure 4. The magnification of a MN formed next to a QDM is shown in panel (f) of figure 4. Increasing the substrate temperature to 340 °C and 360 °C (sample B2 and B3, respectively) during the Ga MN deposition increases the fraction of MNs formed on top of the QDMs (panels (b) and (c) of figure 4). Magnification of a MN formed on top of a QDM is reported in panel (g) of figure 4. The behavior can be clearly observed in figure 5, in which the density of Ga MN formed next and on top of QDM is reported. At 320 °C about 78.0% of the MNs

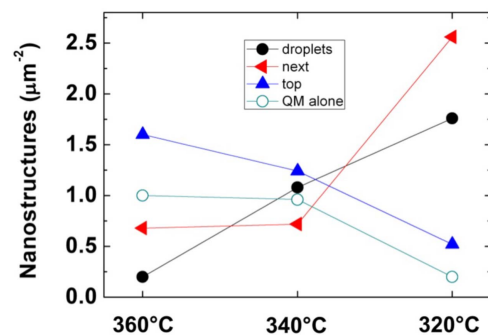


Figure 5. Density in nanostructures μm^{-2} of QDMs (empty circles) and isolated MNs (black circles), of MN formed next to (red triangles) and on top of QDM (blue triangles) as a function of Ga deposition temperature.

forms next to a QDM and only 15.8% on top, while increasing substrate temperature during Ga deposition to 360 °C resulted in a reduction of MNs formed next to a QDM to 20.7% and in an increase of MN formed on top of a QDM to 48.8%. Finally, increasing the flux of Ga from 0.03 to 0.05 ML s^{-1} (sample C, figure 4 panel (d)) preserves the preferential formation on top but better matches the density between Ga MNs and QDMs. As described in [30], larger Ga flux during the Ga droplet deposition results in a increased density of the MNs on the surface. In this sample the match between the density of QDMs and MNs is achieved by increasing the substrate temperature (step necessary to position the MNs on top of QDMs) and increasing the Ga flux. As

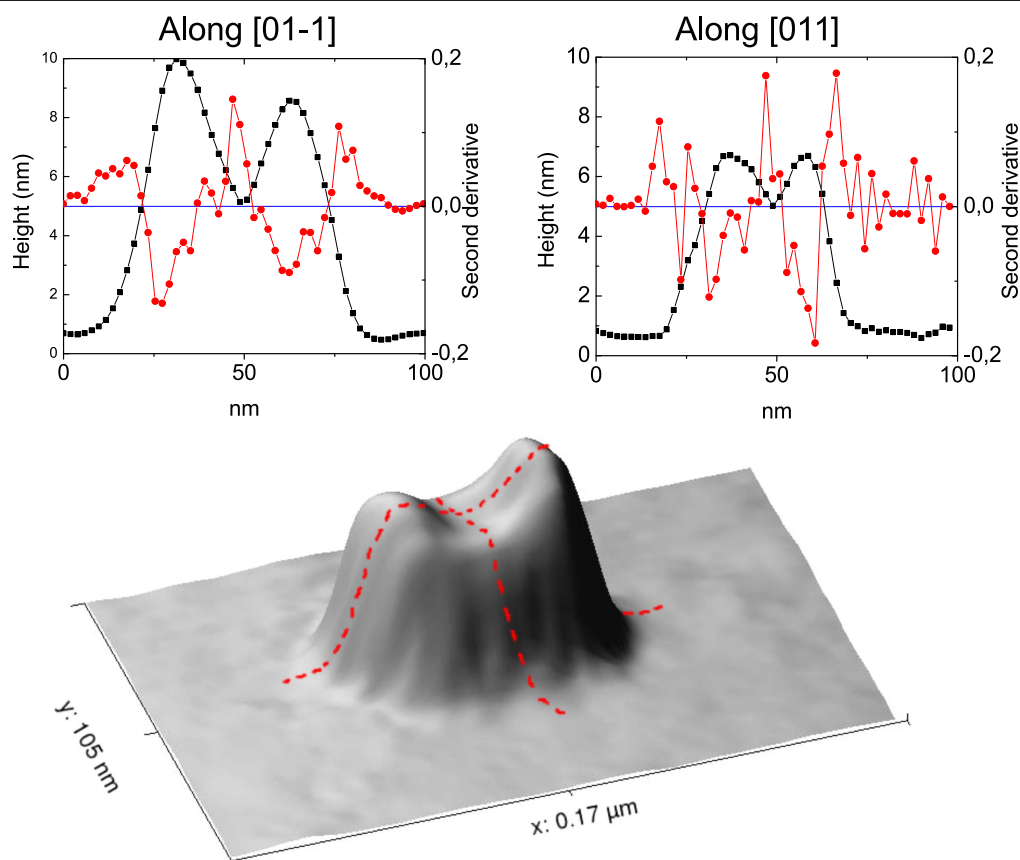


Figure 6. Upper panels: profile (black) and second derivative (red line) calculated along the red dashed lines of the AFM scan of a single QDM (lower panel).

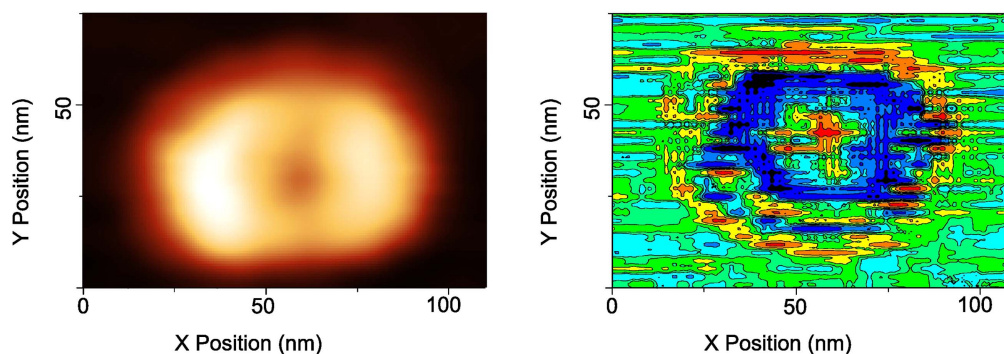


Figure 7. High resolution AFM scan of a typical QDM (left panel) and the result of the bidimensional Laplacian operator on the same area (right panel). Blue/deep blue and orange/red areas denotes convex and concave regions, respectively.

final result, on this samples 67.8% of the MNs formed on top of a QDM and only 14.7% next to a QDM.

In order to explain the positioning of the Ga MNs, it is necessary to consider that concave surfaces are energetically favorable for the nucleation of a droplet, as reported in the literature (e.g. [40, 41]). To estimate the concavity on a typical QDM, we calculated second derivative along [01-1] and [011] directions as reported in figure 6. The maximal values, corresponding to larger concavity, are reached near the border between the substrate and the nanostructure, and at the center of the QDM in the valley between the two dots.

The radius of curvature is approximately 12 nm at the base along [01-1] direction, and approximately 6 nm in the center of the QDM structure.

The two-dimensional mapping of the curvature can be obtained via the bidimensional Laplacian operator on the area of a single typical QDM (figure 7). It shows maxima all along the rim of the nanostructure and in its center. It is interesting to notice that the nucleation next to a nanostructure is preferentially along the major axis of the QDM, as can be observed in panel (b) of figure 4. In fact, on our samples we found evidence of the nucleation of MNs next to a QDM

along the major axis for all the nanostructures except one. This behavior was already described and explained in [42] with the preferential nucleation on (111)B surfaces.

In order to explain the different preferential position for nucleation at different substrate temperatures (top of or next to QDM), we have to consider that the maximum value of the second derivative is reached at the center of the QDMs. At the rim of each nanostructure, the surface is concave moving along radial direction, but moving perpendicularly to radial direction the surface is convex. In the valley between the two dots forming the QDM, the surface is concave in any direction, thus making this position more favorable for nucleation. But to reach this area at the top of the QDM, the Ga atoms have to overcome the atomic steps along the external walls of the QDM structure. The possibility of adatoms jumping up an ascending step was reported in scientific literature as the result of two processes, the capture at a step-edge site and the successive detachment to the upper terrace [43–45]. Because the second step of this process is thermally activated, the increasing in substrate temperature will increase the probability for the Ga adatoms to reach the upper part of the QDM structure. This model could explain the relation between the substrate temperature during the MN deposition and their final position next to or on top of the QDM.

3. Conclusions

A hybrid metal–semiconductor nanosystem for the generation of THz radiation, based on the fabrication of GaAs quantum molecules-Ga metal MNs complexes through a self assembly approach, is proposed. The role of the growth parameters, the substrate temperature and the Ga flux, for the alignment and the precise matching of MNs next to or on top of the QDMs was studied. Increasing the substrate temperature during the deposition of the Ga MNs allows the fine tuning on the positioning of the metallic droplets, resulting in the possibility to deposit a large fraction of the MNs either next to (up to 78.0%) or on top of (up to 67.8%) the QDMs. This permits a change to the relative orientation of the MN with respect to the dipolar moments of the QDM, maximizing the plasmonic resonance effects of the THz emission. Increasing the Ga flux during the deposition of the Ga MNs allows a match of the density of the MNs with the one of QDMs, thus increasing the number of nanostructures suitable for plasmonic resonance effects. The electronic structure of a typical QDM was evaluated on the base of the morphological characterizations performed by atomic force microscopy and cross sectional scanning electron microscopy, and the predicted results confirmed by μ -PL experiments, showing that the Ga metal nanoparticle-GaAs quantum molecule complexes are suitable for THz generation from intraband transition.

Acknowledgments

The authors acknowledge support from project FEMTOTERA (FP7 Concert-Japan). The authors declare no competing financial interest.

ORCID iDs

Sergio Bietti  <https://orcid.org/0000-0001-5775-0687>

Caterina Vozzi  <https://orcid.org/0000-0002-0212-0191>

References

- [1] Sirtori C 2002 Applied physics: bridge for the terahertz gap *Nature* **417** 132–3
- [2] Reimann K 2007 Table-top sources of ultrashort THz pulses *Rep. Prog. Phys.* **70** 1597
- [3] Köhler R, Tredicucci A, Beltram F, Beere H E, Linfield E H, Davies A G, Ritchie D A, Iotti R C and Rossi F 2002 Terahertz semiconductor-heterostructure laser *Nature* **417** 156–9
- [4] Lee A W M, Qin Q, Kumar S, Williams B S, Hu Q and Reno J L 2006 Real-time terahertz imaging over a standoff distance (25 meters) *Appl. Phys. Lett.* **89** 141125
- [5] Davies A G, Burnett A D, Fan W, Linfield E H and Cunningham J E 2008 Terahertz spectroscopy of explosives and drugs *Mater. Today* **11** 18–26
- [6] Fitzgerald A J, Cole B E and Taday P F 2005 Nondestructive analysis of tablet coating thicknesses using terahertz pulsed imaging *J. Pharmaceutical Sci.* **94** 177–83
- [7] Woodward R M, Wallace V P, Pye R J, Cole B E, Arnone D D, Linfield E H and Pepper M 2003 Terahertz pulse imaging of ex vivo basal cell carcinoma *J. Investigative Dermatology* **120** 72–8
- [8] Brzozowski M J and Singh M R 2017 Photoluminescence quenching in quantum emitter, metallic nanoparticle, and graphene hybrids *Plasmonics* **12** 1021–8
- [9] Low T and Avouris P 2014 Graphene plasmonics for terahertz to mid-infrared applications *ACS Nano* **8** 1086–101
- [10] Singh M R, Guo J, Cid J M J and De Hoyos Martinez J E 2017 Control of fluorescence in quantum emitter and metallic nanoshell hybrids for medical applications *J. Appl. Phys.* **121** 094303
- [11] Singh M R, Sekhar M C, Balakrishnan S and Masood S 2017 Medical applications of hybrids made from quantum emitter and metallic nanoshell *J. Appl. Phys.* **122** 034306
- [12] Guo J, Black K, Hu J and Singh M 2018 Study of plasmonics in hybrids made from a quantum emitter and double metallic nanoshell dimer *J. Phys.: Condens. Matter* **30** 185301
- [13] Sakai K and Tani M 2005 *Introduction to Terahertz Pulses* (Berlin: Springer) pp 1–30
- [14] Carreño F, Antón M A, Melle S, Calderón O G, Cabrera-Granado E, Cox J, Singh M R and Egatz-Gómez A 2014 Plasmon-enhanced terahertz emission in self-assembled quantum dots by femtosecond pulses *J. Appl. Phys.* **115** 064304
- [15] Roskos H G, Nuss M C, Shah J, Leo K, Miller D A B, Fox A M, Schmitt-Rink S and Köhler K 1992 Coherent submillimeter-wave emission from charge oscillations in a double-well potential *Phys. Rev. Lett.* **68** 2216–9
- [16] Hohenester U, Troiani F, Molinari E, Panzarini G and Macchiavello C 2000 Coherent population transfer in coupled semiconductor quantum dots *Appl. Phys. Lett.* **77** 1864–6
- [17] Chikyow T and Koguchi N 1990 MBE growth method for pyramid-shaped GaAs micro crystals on ZnSe(001) surface using Ga droplets *Japan. J. Appl. Phys.* **29** L2093–5
- [18] Koguchi N, Ishige K and Takahashi S 1993 New selective molecular-beam epitaxy growth method for direct formation of GaAs quantum dots *J. Vac. Sci. Technol. B* **11** 787
- [19] Kuroda T, Mano T, Ochiai T, Sanguinetti S, Sakoda K, Kido G and Koguchi N 2005 Optical transitions in quantum ring complexes *Phys. Rev. B* **72** 8

- [20] Somaschini C, Bietti S, Koguchi N and Sanguinetti S 2009 Fabrication of multiple concentric nanoring structures *Nano Lett.* **9** 3419–24
- [21] Ohta K, Kojima T and Nakagawa T 1989 Anisotropic surface migration of Ga atoms on GaAs (001) *J. Cryst. Growth* **95** 71–74
- [22] Somaschini C, Bietti S, Fedorov A, Koguchi N and Sanguinetti S 2010 Concentric multiple rings by droplet epitaxy: fabrication and study of the morphological anisotropy *Nanoscale Res. Lett.* **5** 1865–7
- [23] Yamagiwa M, Mano T, Kuroda T, Tateno T, Sakoda K, Kido G, Koguchi N and Minami F 2006 Self-assembly of laterally aligned GaAs quantum dot pairs *Appl. Phys. Lett.* **89** 113115
- [24] Wang Z M, Holmes K, Mazur Y I, Ramsey K A and Salamo G J 2006 Self-organization of quantum-dot pairs by high-temperature droplet epitaxy *Nanoscale Res. Lett.* **1** 57–61
- [25] Wu J, Shao D, Dorogan V G, Li A Z, Li S, DeCuir E A, Omar Manasreh M, Wang Z M, Mazur Y I and Salamo G J 2010 Intersublevel infrared photodetector with strain-free GaAs quantum dot pairs grown by high-temperature droplet epitaxy *Nano Lett.* **10** 1512–6
- [26] Tordova D, Patrini M, Tognini P, Stella A, Cheyssac P and Kofman R 1999 Ellipsometric study of optical properties of liquid Ga nanoparticles *J. Phys.: Condens. Matter* **11** 2211
- [27] Wu P C, Kim T-H, Brown A S, Losurdo M, Bruno G and Everitt H O 2007 Real-time plasmon resonance tuning of liquid Ga nanoparticles by *in situ* spectroscopic ellipsometry *Appl. Phys. Lett.* **90** 103119
- [28] Bollani M *et al* 2014 Ordered arrays of embedded Ga nanoparticles on patterned silicon substrates *Nanotechnology* **25** 205301
- [29] Ohtake A, Kocán P, Nakamura J, Natori A and Koguchi N 2004 Kinetics in surface reconstructions on GaAs(001) *Phys. Rev. Lett.* **92** 236105
- [30] Heyn C, Stemmann A, Schramm A, Welsch H, Hansen W and Nemcsics Á 2007 Regimes of GaAs quantum dot self-assembly by droplet epitaxy *Phys. Rev. B* **76** 1–4
- [31] Mano T, Abbarchi M, Kuroda T, Mastrandrea C A, Vinattieri A, Sanguinetti S, Sakoda K and Gurioli M 2009 Ultra-narrow emission from single GaAs self-assembled quantum dots grown by droplet epitaxy *Nanotechnology* **20** 395601
- [32] Adorno S, Bietti S and Sanguinetti S 2013 Annealing induced anisotropy in GaAs/AlGaAs quantum dots grown by droplet epitaxy *J. Cryst. Growth* **378** 515–8
- [33] Califano M and Harrison P 2000 Presentation and experimental validation of a single-band, constant-potential model for self-assembled InAs/GaAs quantum dots *Phys. Rev. B* **61** 10959–65
- [34] Zhang W, Govorov A O and Bryant G W 2006 Semiconductor–metal nanoparticle molecules: hybrid excitons and the nonlinear fano effect *Phys. Rev. Lett.* **97** 146804
- [35] Borri P, Langbein W, Schneider S, Woggon U, Sellin R L, Ouyang D and Bimberg D 2001 Ultralong dephasing time in GaAs quantum dots *Phys. Rev. Lett.* **87** 157401
- [36] Abbarchi M, Kuroda T, Mano T, Sakoda K, Mastrandrea C A, Vinattieri A, Gurioli M and Tsuchiya T 2010 Energy renormalization of exciton complexes in GaAs quantum dots *Phys. Rev. B* **82** 201301
- [37] Heyn C, Stemmann A, Schramm A, Welsch H, Hansen W and Nemcsics Á 2007 Regimes of GaAs quantum dot self-assembly by droplet epitaxy *Phys. Rev. B* **76** 203105
- [38] Bietti S, Somaschini C, Koguchi N, Frigeri C and Sanguinetti S 2011 Self-assembled GaAs local artificial substrates on Si by droplet epitaxy *J. Cryst. Growth* **323** 267–70
- [39] Ohtake A 2008 Surface reconstructions on GaAs(001) *Surf. Sci. Rep.* **63** 295–327
- [40] Fletcher N H 1958 Size effect in heterogeneous nucleation *J. Chem. Phys.* **29** 572
- [41] Qian M and Ma J 2012 The characteristics of heterogeneous nucleation on concave surfaces and implications for directed nucleation or surface activity by surface nanopatterning *J. Cryst. Growth* **355** 73–7
- [42] Elborg M, Noda T, Mano T, Jo M, Sakuma Y and Sakoda K 2013 Self-assembly of Ga droplets attached to GaAs quantum dots *J. Cryst. Growth* **378** 53–6
- [43] Tsong T T and Fu T-Y 1997 Diffusion and elementary atomic processes at steeped surfaces *Prog. Surf. Sci.* **53** 233–9
- [44] Kyuno K and Ehrlich G 1997 Step-edge barriers: truths and kinetic consequences *Surf. Sci.* **394** L179–87
- [45] Antczak G and Ehrlich G 2010 *Surface Diffusion: Metals, Metal Atoms, and Clusters* (Cambridge: Cambridge University Press)